DETRITAL APATITE TRACE-ELEMENT COMPOSITIONS: A ROBUST NEW TOOL FOR MINERAL EXPLORATION

Mao Mao[1], Alexei S. Rukhlov[2], Stephen M. Rowins[1,2], Jody Spence[1], and Laurence A. Coogan[1]

1: School of Earth and Ocean Sciences, University of Victoria, 3800 Finnerty Road, Victoria, British Columbia, V8P 5C2
2: British Columbia Geological Survey, Ministry of Energy and Mines, 1810 Blanshard Street, Victoria, British Columbia, V8W 9N3

Ministry of Energy and Mines

University of Victoria
British Columbia • Canada

MEM - UVic Partnership - Energy and Minerals Projects

For More Information:
(306) 262-3110, mao_11313@hotmail.com
(250) 952-0396, Alexei.Rukhlov@gov.bc.ca

Recommended citation:
Mao, M., Rukhlov, A.S., Rowins, S.M., Spence, J., Coogan, L.A., 2015. Detrital apatite trace-element compositions: A robust new tool for mineral exploration. British Columbia Ministry of Energy and Mines, British Columbia Geological Survey GeoFile 2015-09.

ABSTRACT

Apatite from different deposits, including alkalic porphyry Cu-Au, porphyry Cu-Au, porphyry Cu-Mo, porphyry Mo, porphyry-related breccia Cu-Au, iron oxide copper gold (IOCG), orogenic Au, Au-Co skarn, W skarn, orogenic Ni-Cu deposits and carbonatites, along with apatites from unmineralized rocks, have been analyzed by electron microprobe (EMPA) and laser-ablation inductively coupled plasma mass spectrometry (LA-ICPMS). Selected trace elements (Mg, V, Mn, Sr, Y, La, Ce, Eu, Dy, Yb, Pb, Th and U) are used for discriminant analysis of apatite from different deposit and rock types. Our results show that apatites from the different deposits can be distinguished from apatites in carbonatites and unmineralized rocks. The apatites from mineral deposits are characterized by higher Ca and lower total contents of trace elements that partition onto the Ca sites (rare earth elements (REE), Y, Mn, Sr, Pb, Th, U) than apatites from unmineralized rocks and carbonatites. Apatites from different types of deposits have distinct trace-element compositions that are readily discriminated by the discriminant functions. Apatite from carbonatites has the highest Sr (~2000-10000 ppm), Ba (~5-100 ppm), and Nb (~1-5 ppm) contents, and the lowest W contents (<0.5 ppm) and weak Eu anomalies (Eu/Eu* ~0.9-1.1); apatite from IOCG deposits has negative Eu anomalies (Eu/Eu* ~0.2-0.45) and low Mn contents (<300 ppm); apatites from porphyry Cu-Au and Cu-Mo deposits have the highest Mn contents in this study (1000-10000 ppm) and very strong negative Eu anomalies (Eu/Eu* = ~0.2-0.5); apatite from alkalic porphyry Cu-Au deposits has the highest V contents (~50-400 ppm); and apatites from orogenic Ni-Cu, porphyry-related Cu-Au breccia, and Au-Co skarn deposits have very low total impurity cations. Our findings suggest that trace elements in apatite can be used as effective indicators for mineral exploration.

INTRODUCTION

Apatite is a widespread accessory mineral and incorporates significant quantities of a wide range of trace elements (e.g., Na, Mg, Mn, Fe, Sr, Y, Ba, REE, Pb, Th, U, V, As, Si and S). Previous studies have shown that apatite trace-element compositions can be used to discriminate different types of granites (Sha et al., 1999), carbonatites and Iherzolites (Belousova et al., 2002), and track magmatic and hydrothermal processes associated with the formation of porphyry Cu-Mo-Au deposits (Cao et al., 2011; Bouzari et al., 2011). Here we show that apatite trace-element compositions can be used to discriminate between apatites formed in association with mineral deposits versus unmineralized rocks and to identify major deposit types.

Table 1. Classification of apatite samples and number of analyses in this study. Apatites from mineral deposits were all selected from mineralized zones.

Classification	Deposit name	Rock samples	Analyses	Total analyses
Alkalic porphyry Cu-Au	DOBBIN (ALPS), BC	4	59	145
	MOUNT POLLEY (CARBIDO-BELL), BC	2	48	
	SHAKI (RED GOLD), BC	3	38	
Porphyry Cu-Au	ARMESS (SOUTH ZONE), BC	2	33	33
Porphyry-related breccia Cu-Au	MILLA (L.1576) (ROCKLAND GROUP), BC	1	34	34
Porphyry Cu-Mo	GIBRALTAR, BC	1	2	55
	HIGHMONT (HIGHMONT MINE), BC	1	20	
	HIGHLAND VALLEY COPPER (VALLEY), BC	1	6	
	LORNEX (LORNEX MINE), BC	1	16	
	ENDAKO (ENDAKO MINE), BC	1	7	
Porphyry Mo	ROSS MOUNTAIN (BIPHOMC), BC	1	11	63
	CASSIAR MOLY, BC	1	24	
	BRENDA (BRENDA MINE), BC	1	23	
IOCG-Breccia	WERNECKE, YUKON	4	44	44
IOCG-Kiruna type	ADIVARI, CHINA	5	37	267
	GREAT BEAR (RAINY LAKE PLUTON), NWT	1	13	
	OURANGO, MEXICO	7	217	
Orogenic Ni-Cu	JASON, BC	1	28	28
Orogenic Au	CONGRESS (LOU), BC	1	12	56
	DENTONIA (DENTONIA MINE), BC	1	2	
	DEMBE, SASKATCHEWAN	5	34	
	KIRKLAND LAKE, ONTARIO	1	8	
	MAYKARI, AUSTRALIA	1	12	
Au-Co skarn	RAIDNE, BC	1	15	15
Cu skarn	LITTLE BITTLE (LITTLE BILLY), BC	1	1	1
Pb-Zn skarn	GOLD CAMPOS, BC	1	1	1
W skarn	MOLLY (L.1422) (MOUNTKENTY), BC	1	26	26
	OTAGUARARA, AUSTRALIA	1	0	
Epithermal Au-Ag	ONIOLA (OPEOGNA/HARMONY), BC	1	2	9
	CRIPPLE CREEK, COLORADO	1	7	
Carbonatite	29 INTRUSIVE COMPLEXES WORLDWIDE	31	73	73
MORB	SOUTHWEST INDIAN RIDGE (ATLANTIS BANK)	2	19	52
	MID-ATLANTIC RIDGE	2	8	
	EAST PACIFIC RISE (MESS DEEP)	8	13	
Unmineralized	KIRKLAND LAKE, ONTARIO (Syenite rocks)	1	16	248
	BELL STARR (Alkali syenite gneiss), BC	1	1	
	THEBAIDE CREEK PLUTON, BC (Syenite rocks)	1	3	
	BEAVER COVE PLUTON, BC (Syenite rocks)	1	9	
Other	137 MINE DISCOVERY, MADAGASCAR (Pegmatite-Standard)	1	230	230

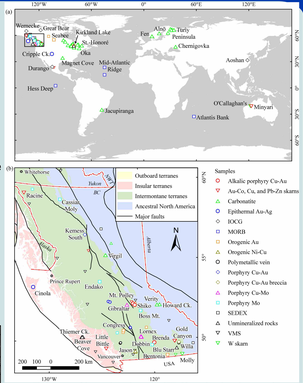

Figure 1. The locations of the samples in this study. a) World map; box shows locations of Figure 1b. b) British Columbia map. The symbols on both maps represent deposit types, samples from which were examined in this study. The larger symbols represent samples that yielded apatite investigated in this study.

ANALYTICAL METHODS

Major and some trace elements were determined by a fully automated Cameca SX50 Electron Microprobe (EMPA) equipped with four wavelength-dispersive spectrometers at the Department of Earth, Ocean and Atmospheric Sciences, University of British Columbia. Trace element abundances were analyzed using a New Wave UP-213 laser ablation system coupled to Thermo X-Series II (X7) quadrupole inductively coupled plasma mass spectrometer (LA-ICPMS), with helium used as the carrier gas, at the School of Earth and Ocean Science, University of Victoria. Calcium concentrations (2 sigma ~1%) determined by EMPA for most of the apatites was used as the internal standard for the LA-ICPMS calibration. NIST 611, 613, and 615 glass were used as the external calibration standards. Natural apatite crystals from Madagascar and Durango (Young et al., 1969; Thomson, 2010) have been used to determine the effect of the difference in matrix, and to determine experimental accuracy and precision. Based on NIST613, Durango and Madagascar apatite, the precision (2 sigma) for elements with concentration ranging from tens to several hundred ppm are < 10% for Mn, Sr, La, Ce, and Pr; from 10% to 20% for Y, Pb, Th, U and the rest of REE; and from 20% to 30% for Mg and V. During the experimental sessions that used decreased laser energy, the detection limits are < 60 ppm for Mg, < 30 ppm for Mn, < 15 ppm for V, < 5 ppm for La, Ce, < 2 ppm for the rest of elements.

RESULTS

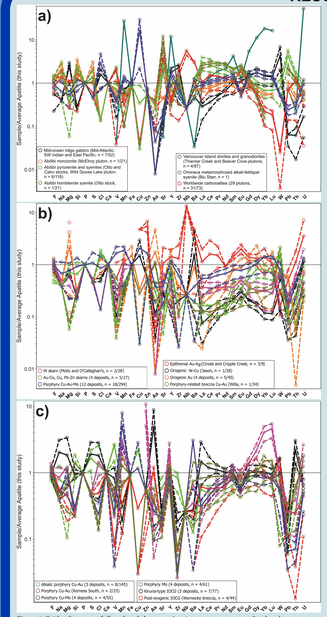

Figure 2. Spider diagrams of all analyzed elements. Apatite contents are normalized to the average apatite contents in this study. The solid lines are the median value, and the dashed lines are the first and third quartile: a) Apatite from unmineralized groups; b) Apatite from mineral deposits except IOCG; c) Apatite from different porphyries and IOCG deposits. These figures demonstrate large variations of the trace element abundances in apatites from different deposit and rock types.

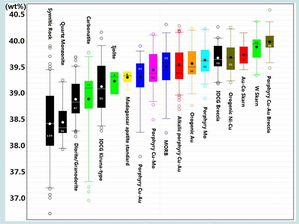

Figure 3. Ca contents of apatite. Line: median value; Black dot: mean value; Box: interquartile range (25th-75th percentile); Whiskers: 5th to 95th percentiles; Open circle: <5th and >95th percentile values. The apatites from mineral deposits have higher Ca and lower total contents of trace elements that partition onto the Ca sites (REE, Y, Mn, Sr, Pb, Th, U) than apatites from unmineralized rocks and carbonatites.

DISCRIMINANT PROJECTION ANALYSIS

We have performed the discriminant analysis on trace-element data from apatites to determine the optimal discrimination of apatites from different deposit and rock types that could be used for mineral exploration. To do this, we used discriminant projection analysis (DPA) to devise an optimum set of rules to classify apatite compositions into one of a set of predefined groups by projecting multivariate data into a lower dimensional space to show the best separation between the groups. These discriminant functions or projections (DP1, DP2, etc.) are linear combinations of the original variables that maximize the differences between the predefined groups, which allow the samples to be plotted in the discriminant space so that group separation can be visualized and investigated. The DPA also indicates which of the selected variables are most important for determining maximum group separation. To achieve this, we performed the DPA on Log10-transformed LA-ICPMS data on apatite compositions using ioGAS® software. To statistically outline samples within each group on the discrimination diagrams, we used robust contours of constant Mahalanobis distance (MD), which is a measure of central tendency of the multivariate data that takes into account the shape of the data with an outlier cutoff of 0.95 percentile of the chi-squared distribution (De Maesschalck et al., 2000), calculated in ioGAS® software. The element combinations for each DPA calculation were chosen based on individual element contributions to determining the maximum separation between the groups in the discriminant space.

Step I: Ore deposits versus Unmineralized rocks versus Carbonatites

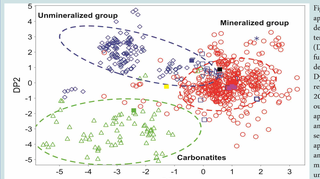

Figure 4. Discrimination diagram for apatite from carbonatites, various ore deposits, and unmineralized rocks in terms of the first discriminant function (DP1) versus the second discriminant function (DP2). DP1 and DP2 were determined by using Mn, Sr, Y, La, Ce, Eu, Dy, Yb, Pb, Th and U. The solid squares represent literature data (Belousova et al., 2002; Cao et al., 2011) that we used to test our discrimination diagrams. The three apatite groups (carbonatite, mineralized and unmineralized) are successfully separated from each other, with only apatite from unmineralized dioritic rocks and MORBs overlapping with those from mineral deposits. The apatites from unmineralized diorites can be discriminated by their relatively high Cl contents (~0.12-2 wt%) and negative Eu anomalies (~0.05-0.3), and the apatites from MORB can be discriminated by their relatively high Zr contents (~2-10 ppm) (See Figure 2 and Figure 11a).

Table 2. Structure coefficients determined from the discrimination of mineralized, unmineralized and carbonatite groups (Figure 4). The values indicate that Sr, Eu, Yb and Yb are the most important contributors to the discriminant functions.

Structure Coefficients	DP1	DP2
Mn_ppm	0.09442	0.1262
Sr_ppm	0.8428	-0.09958
Y_ppm	0.2419	0.4944
La_ppm	-0.3299	0.2676
Ce_ppm	-0.4645	0.2185
Eu_ppm	-0.7168	0.1134
Dy_ppm	0.0865	0.3529
Yb_ppm	0.4123	0.4798
Pb_ppm	-0.7599	0.4943
Th_ppm	-0.1281	0.127
U_ppm	0.3111	0.4423
Group		Count
Mineralized		491
Unmineralized		159
Carbonatite		71
Overall		721

Step II: Discrimination of general ore deposits (6 groups)

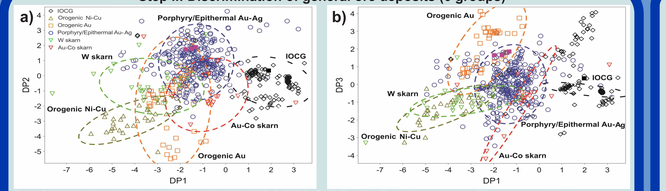

Figure 5. Discrimination diagrams for apatite from different ore deposits by using Mn, Sr, Y, Ce, Eu, Dy, Yb, Th and U. a) The first discriminant function (DP1) versus the second discriminant function (DP2), and b) The DP1 versus the third discriminant function (DP3). The solid squares represent literature data that we use to test our discrimination diagrams. The diagrams discriminate most of apatite data from IOCG deposits and W skarns (together with orogenic Ni-Cu) from orogenic Au and Au-Co skarn deposits.

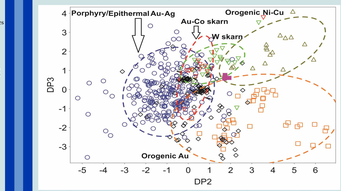

Figure 6. Discrimination diagram for apatite from different ore deposits in terms of the DP2 versus the DP3 which are determined by using Mg, Mn, Sr, Y, Ce, Eu, Dy, Yb, Th and U. Note, the solid squares represent literature data that we use to test our discrimination diagrams. Most of apatites from orogenic Au and orogenic Ni-Cu groups can be separated from other deposit types.

Table 3. Structure coefficients determined from the discrimination of general ore deposits (Figure 5 and 6, Tables left to right, respectively). The values indicate that Mn, Ce, Yb and Th provide the largest contributions to discriminant functions in Figure 5; and Y, Yb and Th are the most important contributors to discriminant functions in Figure 6.

Structure Coefficients	DP1	DP2	DP3
Mn_ppm	-0.6908	0.4527	0.2023
Sr_ppm	-0.1203	0.06925	7.00E-04
Y_ppm	0.5157	0.5186	0.432
Ce_ppm	0.7515	0.2388	-0.09948
Eu_ppm	0.0445	0.3401	0.5333
Dy_ppm	0.4415	0.4093	0.5776
Yb_ppm	0.3972	0.6892	0.261
Th_ppm	0.6066	0.1183	-0.4695
U_ppm	-0.07949	0.2507	-0.3307
Group			Count
IOCG			119
Orogenic Ni-Cu			28
Orogenic Au			43
Porphyry/Epithermal Au-Ag			313
W skarn			28
Au-Co skarn			17
Overall			548

Structure Coefficients	DP2	DP3
Mg_pct	0.1836	-0.1639
Mn_ppm	-0.1781	-0.2369
Sr_ppm	-0.015	0.04286
Y_ppm	-0.4815	-0.5134
Ce_ppm	-0.3422	0.1632
Eu_ppm	-0.178	-0.5358
Dy_ppm	-0.3357	-0.6365
Yb_ppm	-0.6338	-0.3907
Th_ppm	-0.2793	0.5082
U_ppm	-0.2395	0.3685
Group		Count
IOCG		101
Orogenic Ni-Cu		16
Orogenic Au		43
Porphyry/Epithermal Au-Ag		270
W skarn		26
Au-Co skarn		13
Overall		469

Step IIIa Discrimination of different porphyries and skarns (7 groups)

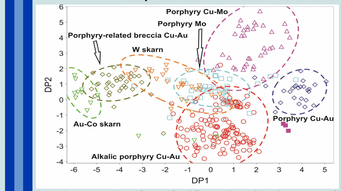

Figure 7. Discrimination diagram for apatite from different porphyry and skarn deposits in terms of the DP1 versus DP2 which are determined using Mg, Mn, Sr, Y, Ce, Eu, Yb, Th and U. The solid squares represent literature data that we use to test our discrimination diagrams. Apatite from alkalic porphyry Cu-Au group is distinguished from other groups, as well as porphyry Cu-Mo and porphyry Mo are separated from Au-Co skarn and porphyry-related breccia Cu-Au, and most of the porphyry Cu-Au deposits.

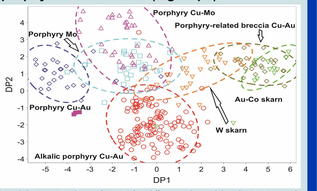

Figure 8. Discrimination diagram for apatite from different porphyry and skarn deposits in terms of DP1 and DP2 which are determined using Mg, Mn, Sr, Y, Ce, Eu, Yb, Th and U. The solid squares represent literature data that we use to test our discrimination diagrams. Apatite from alkalic porphyry Cu-Au group is distinguished from other groups, as well as porphyry Cu-Mo and porphyry Mo are separated from Au-Co skarn and porphyry-related breccia Cu-Au, and most of the porphyry Cu-Au deposits.

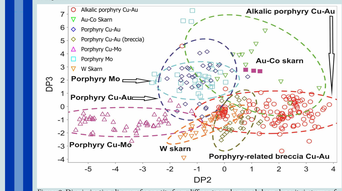

Figure 9. Discrimination diagram for apatite from different porphyry and skarn deposits in terms of DP2 and DP3 which are determined from Mg, Mn, Sr, Y, Ce, Eu, Dy, Pb and U. The solid squares represent literature data that we use to test our discrimination diagrams. Note separation of apatite data from porphyry Cu-Mo from other deposit types and porphyry Mo together with porphyry Cu-Au from W skarn, alkalic porphyry Cu-Au and porphyry-related breccia Cu-Au. The three discrimination diagrams (Figure 7-9) separate most of the apatite data from all of the deposit types.

Table 4. Structure coefficients determined from the discrimination of porphyry and skarn groups (Figure 7 - 9. Tables left to right, respectively). The values indicate that Mn, Sr, Eu and Yb provide the largest contributions to discriminant functions in Figure 7; Mn, Eu and Yb contribute the most to discriminant functions in Figure 8; and Mn, Sr, Y and Dy are the most important discriminants in Figure 9.

Structure Coefficients	DP1	DP2
Mg_pct	0.5718	0.1508
Mn_ppm	0.6294	0.6876
Sr_ppm	0.271	-0.5431
Y_ppm	0.0762	-0.235
Ce_ppm	0.5957	-0.1196
Eu_ppm	0.7794	-0.4396
Yb_ppm	0.708	-0.2008
Th_ppm	0.08578	-0.5436
U_ppm	0.2883	-0.2699
Group		Count
Alkalic porphyry Cu-Au		129
Au-Co skarn		13
Porphyry Cu-Au		26
Porphyry-related breccia Cu-Au		33
Porphyry Cu-Mo		38
Porphyry Mo		35
W skarn		26
Overall		300

Structure Coefficients	DP1	DP2
Mg_pct	-0.5761	0.09559
Mn_ppm	-0.6647	0.6163
Sr_ppm	-0.1431	-0.6368
Y_ppm	-0.709	-0.219
Ce_ppm	-0.6259	-0.1518
Eu_ppm	-0.7603	-0.509
Yb_ppm	-0.7806	-0.1599
Pb_ppm	-0.2848	0.0806
Th_ppm	-0.1536	-0.4953
U_ppm	-0.3482	-0.2209
Group		Count
Alkalic porphyry Cu-Au		128
Au-Co skarn		12
Porphyry Cu-Au		32
Porphyry-related breccia Cu-Au		28
Porphyry Cu-Mo		46
Porphyry Mo		30
W skarn		26
Overall		302

Structure Coefficients	DP1	DP2
Mg_pct	-0.3449	0.0845
Mn_ppm	-0.8666	0.1529
Sr_ppm	0.4719	-0.5205
Y_ppm	-0.02199	0.6268
Ce_ppm	-0.1068	0.241
Eu_ppm	0.1747	0.1558
Dy_ppm	-0.06581	0.5721
Pb_ppm	0.0276	0.4757
U_ppm	0.2133	0.3376
Group		Count
Alkalic porphyry Cu-Au		128
Au-Co skarn		12
Porphyry Cu-Au		32
Porphyry-related breccia Cu-Au		28
Porphyry Cu-Mo		46
Porphyry Mo		30
W skarn		26
Overall		302

Step IIIb: Discrimination of different IOCG groups (2 groups)

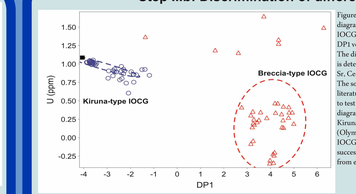

Figure 10. Discrimination diagram for apatite from IOCG deposits in terms of DP1 versus Log U (ppm). The discriminant function is determined using V, Mn, Sr, Ce, Eu, Yb, Pb and Th. The solid squares represent literature data that we use to test our discrimination diagrams. The apatites from Kiruna-type and breccia (Olympic Dam-type) IOCG deposits are successfully discriminated from each other.

Table 5. Structure coefficients determined from the discrimination analysis of IOCG deposits (Figure 10). The values indicate that V, Ce, and Th are the most important contributors to discrimination of these deposits.

Structure Coefficients	DP1
V (ppm)	-0.971
Mn (ppm)	0.3763
Sr (ppm)	-0.391
Ce (ppm)	-0.8173
Eu (ppm)	0.3757
Yb (ppm)	-0.1638
Pb (ppm)	-0.253
Th (ppm)	-0.8979
Group	Count
IOCG (Kiruna-type)	52
IOCG breccia	40
Overall	92

TESTING THE DISCRIMINANT FUNCTIONS

To test the DPA functions determined from the data in this study, literature trace-element data from apatite (Belousova et al., 2002; Cao et al., 2011) have been projected into the discrimination diagrams for each step. Results show that the apatite data from IOCG and porphyry Cu-Mo deposits, carbonatites and unmineralized granitic pluton are all correctly classified in step I, II, and IIIb (Figure 4-6 and10), but the apatite data from Aktogai porphyry Cu-Mo deposit (Kazakhstan; Cao et al., 2011) fall outside the porphyry Cu-Mo field (Figure 7-9). Notably, the Mn contents in apatite from Aktogai porphyry Cu-Mo deposit are lower than those of apatite from porphyry Cu-Mo deposits in this study. The difference may be owing to the different analytical methods (EMPA in Cao et al., 2011 and LA-ICPMS in this study). However, the apatite data from Aktogai deposit fall close to the porphyry Cu-Au deposit, a sub-type of a broad group of porphyry Cu-Au-Mo deposits.

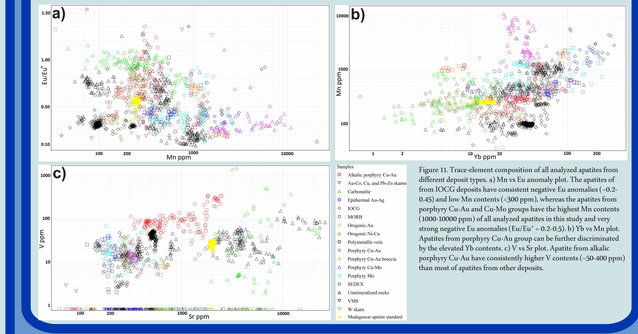

Figure 11. Trace-element composition of all analyzed apatites from different deposit types. a) Mn vs Eu anomaly plot. The apatites of from IOCG deposits have consistent negative Eu anomalies (~0.2-0.45) and low Mn contents (<300 ppm), whereas the apatites from porphyry Cu-Au and Cu-Mo groups have the highest Mn contents (1000-10000 ppm) of all analyzed apatites in this study and very strong negative Eu anomalies (Eu/Eu* ~ 0.2-0.5). b) Yb vs Mn plot. Apatites from porphyry Cu-Au group can be further discriminated by the elevated Yb contents. c) V vs Sr plot. Apatite from alkalic porphyry Cu-Au have consistently higher V contents (<50-400 ppm) than most of apatites from other deposits.

CONCLUSIONS

1. Apatite trace element compositions can be used to robustly differentiate apatites associated with mineralized rocks, carbonatites and unmineralized (country) rocks (Figure. 4).
2. The compositions of apatites associated with mineralization readily differentiate IOCG (Kiruna- and breccia-type), orogenic Ni-Cu, porphyry Cu-Au, Cu-Mo, Mo, and alkalic porphyry Cu-Au, porphyry-related breccia Cu-Au, Au-Co (±Cu, ±Pb-Zn) and W skarns, and orogenic Au deposits (Figure. 5-11).
3. The apatite in mineralized rocks crystallized from hydrothermal fluids containing relatively low concentrations of the elements that partition onto the Ca sites due to relatively low temperatures and pressures causing the decreased mobility of impurities.
4. Compositions of literature apatite data show that apatites can be used as an effective indicator mineral for mineral exploration, and the future precise trace-element data from apatites will further enhance the utility of this method in exploration fields.
5. Our findings can be used to determine the origin of detrital apatite from overburden (e.g., till and alluvial sediments) and thus to use apatite trace-element compositions as a robust exploration tool. This will be especially powerful in the search for concealed carbonatites.

ACKNOWLEDGEMENTS

We appreciate Kathy Gillis (UVic), Barbara John, Graham Nixon (BCGS), Yuanming Pan (University of Saskatchewan), Stuart Thomson (University of Arizona) for loan of some samples, Edith Czech (UBC), Mati Raudsepp(UBC) for their assistance of EMPA, Andre Panteleyev (XDM Geo Consulting) for useful discussion of porphyry deposits, and MEM-UVic Partnership for financial support.

KEY REFERENCES

Belousova, E.A., Griffin, W.L., O'Reilly, S.Y., and Fisher, N.I., 2002, Apatite as an indicator mineral for mineral exploration: trace-element compositions and their relationship to host rock type: Journal of Geochemical Exploration, v. 76, p. 45-69.

Bouzari, F., Hart, C.J.R., Barker, S., and Bissig, T., 2011, Exploration for concealed deposits using porphyry indicator minerals (PIMs): Application of apatite texture and chemistry: In 25th International Applied Geochemistry Symposium, Abstracts, p. 89-90.

Cao, M., Li, G., Qin, K., Seitmuratova, Y., and Liu, Y., 2011, Major and trace element characteristics of apatites in granitoids from central Kazakhstan: Implications for petrogenesis and mineralization: Resource Geology, v. 62, n. 1, p. 63-83.

Maesschalck, R. De, Jouan-Rimbaud, D., and Massart, D.L., 2000, The Mahalanobis distance: Chemometrics and Intelligent Laboratory Systems, v. 50, p. 1-18.

Sha, L.-K., and Chappell, B.W., 1999, Apatite chemical composition, determined by electron microprobe and laser-ablation inductively coupled plasma mass spectrometry, as a probe into granite petrogenesis: Geochimica et Cosmochimica Acta, v. 63, p. 3861– 3881.

Thomson, S.N., 2010, U-Th-Pb dating of apatite: Arizona Laser Chron Center, University of Arizona.

Young, E.J., Myers, A.T., Munson, E.L., and Conklin, N.M., 1969, Mineralogy and geochemistry of fluorapatite from Cerro de Mercado, Durango, Mexico: US Geological Survey Paper, v. 650D, p. 84-93.